High-pressure–temperature phase diagram and the equation of state of beryllium

Amy Lazicki
CEA, DAM, DIF, 91297 Arpajon Cedex, France and Lawrence Livermore National Laboratory, Livermore, California 94551, USA

Agnès Dewaele and Paul Loubeyre
CEA, DAM, DIF, 91297 Arpajon Cedex, France

Mohamed Mezouar
European Synchrotron Radiation Facility, BP 220, F-38043 Grenoble Cedex, France
(Received 9 August 2012; published 30 November 2012)

X-ray diffraction of beryllium in a laser-heated diamond anvil cell provides experimental insight into its behavior at high pressure and temperature. We measure the cold compression of Be in helium and NaCl pressure media up 192 GPa, and its thermal expansion up to 82 GPa and 2630 K. The new measurements form a P-V-T data set which is fit by the Vinet-Debye form to establish a Be experimental equation of state. We compare the results to several theoretical models. The crystal structure of Be is determined up to 205 GPa and 4000 K; no evidence for the predicted high-temperature transition to a cubic phase is found. Finally, the maximum temperature stability of the solid phase along isobaric heating ramps gives a lower bound for the melting curve.

DOI: 10.1103/PhysRevB.86.174118 PACS number(s): 61.50.Ks, 64.30.−t, 65.40.De

The properties of beryllium at high temperature and pressure are important primarily because its light weight and low density coupled with high strength and high thermal conductivity make Be very useful for the defense, aerospace, and nuclear power industries. Of particular recent interest is its potential as a capsule material for inertial confinement fusion (ICF).[1] High laser ablation rate, high thermal conductivity, and stability against Rayleigh-Taylor growth[2] make (doped) Be potentially a better option than the currently employed plastic capsule material. The initial laser pulse in the ICF design will bring the Be capsule to pressures on the order of 2 Mbar and temperatures of 4000 K,[3] the thermodynamic domain covered in this study. The response of the capsule to this initial pulse is an important constraint for theoretical models which attempt to describe the much more extreme conditions achieved during subsequent pulses.

As a subject of theoretical studies, α-Be (hexagonal close packed, hcp, structure) has received a lot of attention because it represents a special case among other divalent metals with its exceptionally high Debye temperature, small Poisson's ratio, and c/a ratio much less than ideal. Also, under pressure Be is predicted to exhibit multiple solid phases which are very close in energy, with their relative stability affected by anharmonic effects at high T.[4–7] There have been some experimental reports of a new high-temperature phase: β-Be, with its structure interpreted as body-centered cubic (bcc)[8,9] or hexagonal,[10] which was later reinterpreted,[11] suggesting a smaller four-atom orthorhombic (distorted hcp) unit cell instead. The stability domain of the β-Be phase was reported to extend from 1530 K to 1560 K (the melting point)[8] at ambient pressure, and from indirect evidence in a large-volume press apparatus it was inferred that the Clapeyron slope of the α-Be to β-Be transition was negative.[12] A tentative stability domain of β-Be, based on these observations, is represented Fig. 1. Theoretically, however, a low-pressure pocket of β-Be cannot be stabilized without strong anharmonic effects, as it is dynamically unstable at low pressure. Instead, a bcc phase is predicted to appear close to the melting line above 100 GPa.[5,6,13,14] Recent experimental studies have seen no evidence for the bcc phase, either at low pressure, or up to 200 GPa at ambient temperature,[15,16] or between 15 and 50 GPa at temperatures up to 2000 K.[17]

High-temperature measurements on Be shown in the literature have so far been limited to the very low pressure regime.[8,12,18,19] Various experimental[18,20] and theoretical[4–7] studies have reported values for thermal expansion at ambient and high pressures.

The goals of this study were to measure an equation of state of Be to high precision, combining the cold compression curve and the thermal expansion; to confirm the stability field of β-Be; to search for the predicted bcc-Be at very high pressure; and to investigate the evolution of the melting curve at very high pressure.

I. EXPERIMENTAL METHODS

The experimental conditions in this study are summarized in Table I and the P-T paths followed are shown in Fig. 1. Three runs (Be + He_1, Be + He_2, and Be + He_3) were dedicated to the accurate measurement of the ambient temperature equation of state (EoS) of beryllium from energy-dispersive single-crystal x-ray diffraction (XRD) on the ID30 beamline at the European Synchrotron Radiation Facility, ESRF (Grenoble, France). Small single crystals ($\leqslant 10$ μm) purchased at Brush-Wellman (99.5% purity) were loaded in membrane diamond anvil cells, with helium as a pressure-transmitting medium. The thickness of the sample chamber was always larger than the dimension of the crystal. The same technique had been used to measure with high accuracy the EoS of other low-Z systems in the 100-GPa range.[22] An average of five reflections were measured in each run; relative uncertainty on the lattice parameter was of the order of 4×10^{-4} Å. The pressure was estimated from the luminescence of a small ruby ball (about 3 μm in diameter) and its quasihydrostatic revised calibration.[21]

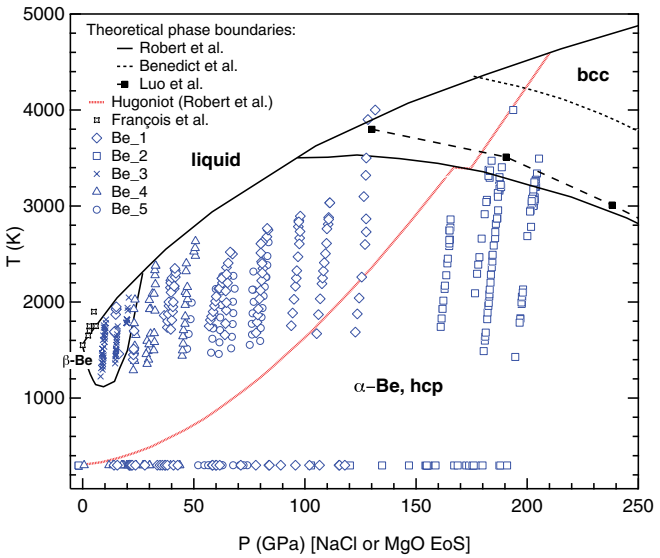

FIG. 1. (Color online) The data points in P-T space, as blue symbols, at which x-ray diffraction patterns have been collected. There was no sign of a bcc or β-Be phase in any of the diffraction patterns. The lines correspond to the phase boundaries predicted by theoretical studies (Refs. 4–6) and the model Hugoniot (Ref. 5).

The remaining runs (Be_1 to Be_5) have been performed using laser heating at the ID27 beamline at the ESRF. Monochromatic X-rays of 0.3738 Å wavelength were focused down to a 2×3 μm^2 spot size, scattered off the samples, and collected on a MAR-CCD bidimensionnal detector. Laser heating was performed simultaneously with diffraction data collection, using two yttrium aluminum garnet (YAG) lasers which provide a maximum power of 200 W. XRD collection times were 20 s to 1 min for the ambient temperature measurements and 5–10 s during laser heating. The heating spot size was adapted to the sample size by focusing (size $\simeq$5 μm) or defocusing (size $\simeq$25 μm) the lasers. Be samples were provided by Goodfellow (99% purity). The temperature was determined from spectral radiometry measurements of the pyrometric signal from an area of $\sim 2 \times 2$ μm^2 in the center of the heating spot, with an average uncertainty of $\sim$100 K. The setup and methods are described elsewhere.[23,24]

For the samples Be_1 to Be_3, pressed pellets of powdered Be were loaded between plates of NaCl in diamond cells. The NaCl was necessary for thermal insulation and to prevent chemical reaction between beryllium and diamond, which form beryllium carbide at high temperature. No reaction between Be and NaCl was observed. In one of these cells (Be_2), the diamonds had pits in their tips of a depth of $\simeq$3 μm to maximize the thickness of the sample and the NaCl thermal insulation. Pressure was determined from the lattice parameters of B1-NaCl (below 35 GPa) or B2-NaCl (above 35 GPa). The cold compression curve of this calibrant has been obtained by merging the most recent P-V measurements.[25,26] The following parameters of the B2-NaCl EoS have been obtained: $V_0 = 45.27$ Å^3/formula unit, $K_0 = 15.2$ GPa, and $K_0' = 6.07$, with a Rydberg-Vinet EoS.[27] The thermal pressure of NaCl has been taken from Ref. 28, which uses a Mie-Grüneisen-Debye approach and is based on a large body of experimental data. Because of the strong temperature gradients away from the heated beryllium, the pressure determination at high temperature has an uncertainty of 5 GPa, approximately.

For Be_4 and Be_5, the thin Be plates were pressed together with $\simeq$1-μm-thick layers of MgO, in close thermal contact with the Be and insulated from the diamonds with plates of NaCl. With this sample assembly, the temperature of the pressure gauge MgO is expected to be close to the temperature of the Be sample. A more accurate pressure determination at high temperature was then made based on the high P-T EoS of MgO.[21]

II. COLD COMPRESSION CURVE

The ambient temperature EoS measurements are reported in Fig. 2 and the data are given in Table II. The volume determination from the single-crystal Be samples compressed in a He medium up to 93 GPa yields the P-V points with the lowest scatter. Nonhydrostatic stresses were negligible, as evidenced by the lack of broadening or distortion of the single crystal spots at high pressure. Samples of Be compressed up to nearly 2 Mbar for the purpose of laser heating were contained in the less hydrostatic NaCl medium. The crystalline phase of Be remained undistorted hcp up to the maximum pressure reached, confirming the conclusions of the most recent XRD studies.[15,16,29]

To provide useful physical parameters (namely, volume V_0, bulk modulus K_0, and its pressure derivative K_0', under ambient conditions) the P-V data points have been fitted by an EoS functional form. We used the Rydberg-Vinet EoS,[27] which expresses the pressure as a function of $X = (V/V_0)^{1/3}$ through

$$P = 3K_0X^{-2}(1 - X)\exp(1.5(K_0' - 1)(1 - X)). \quad (1)$$

TABLE I. Summary of experimental conditions for the different runs performed in this study. The sample chamber drilled in the rhenium gaskets had a diameter lower than half of the diamond culet size. AD, angular-dispersive; ED, energy-dispersive.

Sample name	P_{max} (GPa)	T range (K)	Diamond culet size (μm)	Pressure medium	Pressure calibrant	X-ray method
Be + He_1	21.2	300	150 × 350	He	Ruby (Ref. 21)	ED-XRD
Be + He_2	10	300	500	He	Ruby (Ref. 21)	ED-XRD
Be + He_3	94.7	300	150 × 350	He	Ruby (Ref. 21)	ED-XRD
Be_1	131	300–4000	150 × 350	NaCl	NaCl (see text)	AD-XRD
Be_2	205	300–4000	70 × 300 + pits	NaCl	NaCl (see text)	AD-XRD
Be_3	20.7	300–2047	500	NaCl	NaCl (see text)	AD-XRD
Be_4	51	300–2634	400	NaCl	NaCl/MgO (Ref. 21)	AD-XRD
Be_5	84	300–2623	300	NaCl	NaCl/MgO (Ref. 21)	AD-XRD

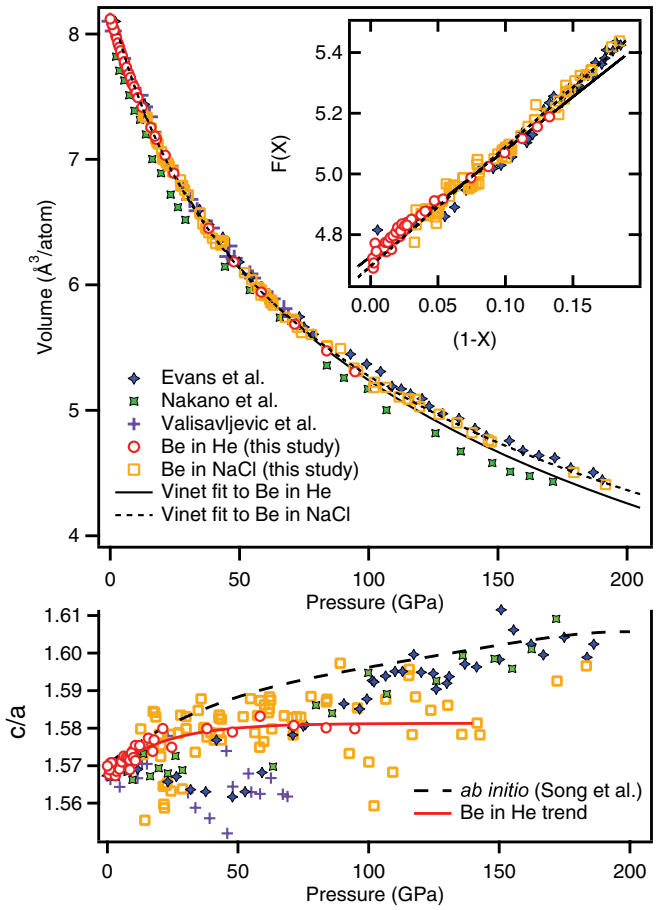

FIG. 2. (Color online) (Top) Summary of 300 K isotherm measured in this study, compared with past experimental results. Error bars associated with measurement uncertainties for the data collected in this study do not exceed the size of the data points. The dispersion of the data is due to the nonhydrostatic stress. The data of Evans *et al.* (Ref. 15) (Be contained in a He medium) are corrected for the new Au pressure scale, and those of Nakano *et al.* (Ref. 16) and Velisavljevic *et al.* (Ref. 29) (no pressure medium) for the new ruby scale (Refs. 21,41). (Inset) Normalized stress vs Eulerian strain terms, from which the bulk modulus K_0 and pressure derivative K_0' were calculated. (Bottom) Evolution of the c/a ratio for these various studies [and an *ab initio* result (Ref. 7)]. The curve shown is a guide for the eye demonstrating the trend in the optimally hydrostatic data. The scatter of the data gives an indication of the degree of uncertainty. The c/a ratio at high temperature found during the heating cycles of the Be in NaCl showed no clear trend in temperature.

V_0 is determined from a fitting of the above equation to the P-V data from the single-crystal Be in He and then fixed at this value for the fitting to the data from Be in NaCl, since the latter does not extend to sufficiently low pressure for a reliable fitted V_0 value. The equation may be reformulated as a normalized stress term, $\ln[H(X)] = \ln[\frac{PX^2}{3(1-X)}]$, and an Eulerian strain term, $(1 - X)$. The results are plotted in the inset of Fig. 2. The data follow a linear trend, the slope of which yields the pressure derivative of the bulk modulus K_0', and the y intercept of the bulk modulus K_0. The fitting parameters are listed in Table III. It can be seen in Fig. 2 that the Be EoS measured in the less hydrostatic NaCl pressure medium (even laser-annealed, as in this case) is slightly stiffer than the extension of the one measured in a He pressure medium, as is well known when nonhydrostatic stresses are present in conventional diffraction geometry in diamond anvil cells.[39]

Also in Fig. 2 are shown the most recent experimental results, for comparison. The data collected by Evans *et al.*[15] were from samples compressed in He with the pressure determined from the calibrated EoS of Au.[40] We have corrected these data points using a more accurate Au EoS,[41] resulting in a shift relative to the published results. The EoS of Evans *et al.* is stiffer than both the EoS measured in this study. The appearance of less hydrostatic conditions in the data set of Ref. 15 could be evidence that the Be sample was bridging the two diamond anvils and thus being uniaxially compressed. High-precision measurements need to be extended to higher pressure to confirm this. Also shown for comparison are the results of Nakano *et al.*[16] and Velisavljevic *et al.*,[29] both compressed without pressure media, using ruby as the pressure calibrant; we updated their ruby scale.[21] The Ref. 29 data agree surprisingly well with the more hydrostatic compression studies.

The evolution of the c/a ratio is shown in the bottom panel of Fig. 2. The degree of scatter in the experimental data gives a good approximation of the average uncertainty for any given data point. The scatter is smallest for the current data obtained with single-crystal XRD in a helium medium and rather large for the current data obtained in an NaCl medium. This may be because single-crystal diffraction peaks are coming from different crystallites with slightly different stress conditions. The different and irregular behavior of c/a in Ref. 15 may be a sign of a change of the stress distribution around 60 GPa in the powdered sample. For the Be in He measurements, the c/a ratio increases approximately linearly up to 1.58 at about 30 GPa, after which it increases only slightly. This variation from the ideal value of 1.633 can be explained in terms of band structure effects. The small c/a ratio has the effect of keeping a set of very flat p-bands below the Fermi level, significantly reducing the total band energy.[42]

The cold compression curve is a sensitive test of the exchange-correlation functionals that best describe the condensed-matter properties of an element. *Ab initio* predictions for the Be EoS are shown in Fig. 3 and parameters are listed in Table III. The EoS provided by Benedict[35] and used here has been slightly modified from the fit presented in Ref. 6, to improve the agreement with the DFT calculations at low pressure. In Refs. 7,13,35, and 38, calculations have been performed with the same approximation of exchange-correlation energy (generalized-gradient approximation, GGA, with the PBE[36] or Perdew[37] functionals). Zero-point vibrations are included in the calculation results presented in Table III. The equilibrium volume obtained with the GGA is within 1% of the experimental V_0 (Table III). In Fig. 3, *ab initio* results are presented in terms of compression $V/V_{0\,ai}$ rather than absolute volume to correct for differing V_0 values. Corrected this way, *ab initio* predictions with GGA follow very closely the Be in NaCl EoS, but are stiffer than the Be in He EoS, a trend which has been noted already for PAW-GGA calculations on several other metals.[43] The Luo *et al.*[4] calculations have been performed within the local density approximation (LDA),

TABLE II. Lattice parameters of α-Be (a and c) at ambient T for the different runs (see Table I). P is in GPa, a and c in Å, V in Å^3/formula unit.

Be in He			Be in NaCl							
P	a	c	MgO V	P	a	c	NaCl V	P	a	c
Be + He_1			**Be_1**				**Be_4**			
0.65	2.284	3.580	33.563	14.3	2.217	3.448	17.428	12.8	2.208	3.489
1.36	2.279	3.575	32.967	15.9	2.199	3.463	17.353	13.7	2.208	3.473
2.13	2.273	3.570	31.204	21.4	2.179	3.409	17.038	17.7	2.190	3.452
3.28	2.266	3.556	31.136	21.6	2.178	3.397	16.886	19.8	2.178	3.438
4.18	2.260	3.548	31.067	21.8	2.178	3.394	16.978	18.5	2.182	3.455
5.53	2.252	3.535	30.911	22.4	2.175	3.403	17.012	18.1	2.183	3.459
6.83	2.244	3.528	30.803	22.8	2.172	3.401	17.051	17.5	2.185	3.463
8.29	2.236	3.515	30.413	24.3	2.168	3.389	16.845	20.4	2.174	3.419
9.60	2.229	3.508	29.387	28.7	2.153	3.367	16.840	20.5	2.175	3.426
10.7	2.223	3.503	27.063	33.6	2.128	3.348	16.595	24.1	2.162	3.412
12.3	2.215	3.490	26.858	34.8	2.123	3.365	16.348	28.0	2.148	3.401
15.7	2.198	3.467	26.680	35.9	2.113	3.355	16.398	27.2	2.155	3.401
17.8	2.189	3.451	26.500	37.0	2.113	3.339	16.391	27.3	2.149	3.393
21.2	2.174	3.435	26.480	37.2	2.112	3.337	16.219	30.1	2.141	3.383
Be + He_2			26.315	38.1	2.110	3.329	16.224	30.1	2.140	3.387
0.54	2.284	3.585	25.915	40.8	2.101	3.312	15.703	39.5	2.104	3.322
1.19	2.279	3.580	25.643	42.7	2.099	3.313	15.502	43.6	2.103	3.316
2.38	2.272	3.564	23.831	58.3	2.055	3.237	15.5	43.6	2.100	3.324
2.98	2.269	3.556	23.674	59.9	2.054	3.238	**Be_5**			
3.51	2.265	3.553	23.814	58.5	2.054	3.261	15.551	42.7	2.099	3.321
4.02	2.262	3.550	23.651	60.1	2.051	3.253	15.546	42.8	2.100	3.326
4.65	2.258	3.544	23.506	61.6	2.047	3.243	15.126	52.0	2.072	3.280
5.48	2.253	3.539	22.683	71.1	2.029	3.202	15.008	54.7	2.063	3.276
6.25	2.248	3.535	22.166	77.9	2.012	3.196	14.896	57.4	2.058	3.259
7.17	2.243	3.527	21.755	83.8	2.002	3.177	14.937	56.4	2.060	3.253
7.80	2.240	3.521	21.736	84.0	2.001	3.177	14.716	62.0	2.044	3.239
8.55	2.236	3.513	21.407	89.1	1.995	3.187	14.696	62.5	2.045	3.246
9.19	2.232	3.512	21.006	95.7	1.978	3.136	14.714	62.1	2.044	3.246
9.96	2.228	3.503	20.652	102.0	1.973	3.076	14.680	62.9	2.044	3.229
10.7	2.225	3.496	20.411	106.6	1.961	3.113	14.396	70.7	2.029	3.212
1.49	2.277	3.577	19.977	115.3	1.946	3.102	14.504	67.7	2.031	3.215
0.79	2.282	3.581	19.968	115.5	1.946	3.105	14.280	74.1	2.017	3.192
0.0	2.286	3.589	19.856	117.9	1.949	3.095	14.338	72.4	2.022	3.200
Be + He_3			**Be_2**							
8.59	2.236	3.509	21.089	94.3	1.986	3.124				
17.3	2.193	3.451	20.643	102.2	1.973	3.099				
24.6	2.162	3.405	20.149	111.8	1.960	3.072				
38.1	2.113	3.338	19.776	119.7	1.945	3.070				
47.9	2.083	3.290	19.442	127.3	1.935	3.066				
58.4	2.054	3.252	19.158	134.2	1.925	3.053				
71.4	2.025	3.202	18.932	140.0	1.918	3.027				
83.7	2.000	3.160	18.698	146.3	1.909	3.019				
94.7	1.980	3.128	18.656	147.4	1.908	3.012				
			17.631	179.4	1.869	2.977				
			17.291	191.6	1.854	2.961				

leading to a different equilibrium volume and exhibiting a divergent P vs $V/V_{0\,ai}$ trend.

III. STABILITY OF THE HCP PHASE

Thin samples of Be were laser heated directly for the high-temperature studies. Well insulated from the diamond surfaces, the Be couples very well with the laser radiation and heating is stable. At high temperature, the Be sample begins to recrystallize, and only isolated single-crystal spots may be seen on the image plate (Fig. 4); generally 2 or 3 spots per peak class. Upon further raising of the temperature, the azimuthal positions of the single-crystal spots on the image plate begin to move at each exposure (see below for further

TABLE III. Rydberg-Vinet[27] EoS fitting parameters for the current data, compared to previous XRD and ultrasonic measurements and to theoretical predictions. Where pressure references in the diamond anvil cell studies have been recalibrated since the publications, the results we report here show the fitting parameters updated with the new calibration.[21,41] Uncertainties on the last digit are between parentheses. The numbers in bold font have been fixed during the fit. LDA, local density approximation; GGA, generalized gradient approximation; PAW, projector augmented wave; pseudo, pseudopotential.

	P range (GPa)	V_0 (Å^3/atom)	K_0 (GPa)	K'_0
This study, Be in He[a]	0–93	8.133(5)	114(1)	3.27(5)
This study, Be in NaCl[a]	12–192	**8.133**	110(2)	3.62(9)
Evans *et al.*, diffraction (Ref. 15)[b]	1–190		115(1)	3.53(3)
Nakano *et al.*, diffraction (Ref. 16)[b]	1–171		100	3.72
Velisavljevic *et al.*, diffraction (Ref. 29)[c]	0–66		100.8	4.388
Ultrasonic (Refs. 30–33)			112(1)[d]	4.6[e]
Luo *et al.* (Ref. 4), Pseudo-LDA [Perdew Zunger (Ref. 34)] (300 K)[b]		7.910	118	3.21
Benedict *et al.* (Refs. 6 and 35), pseudo or all electrons-GGA [PBE (Ref. 36)] (300 K)[a]		8.024	107	3.65
Song *et al.* (Ref. 7), PAW-GGA [PBE (Ref. 36)] (293 K)[a]		8.145	115	3.56
Sin'ko *et al.* (Ref. 13), all electrons-GGA [Perdew (Ref. 37)] (298 K)[a]		8.067	109.4	3.74
Robert and Sollier (Ref. 38), pseudo-GGA [PBE (Ref. 36)] (298 K)[a]		8.128	109.4	3.70

[a]Rydberg-Vinet EoS.
[b]Third-order Birch-Murnaghan EoS.
[c]AP2 EoS.
[d]Isothermal bulk modulus deduced from single-crystal elastic constants. The adiabatic bulk modulus $K_S = (C_{33}(C_{11} + C_{123} - 2C_{13}^2))/(C_{11} + C_{12} - 4C_{13} + 2C_{33})$. The adiabatic to isothermal correction has been done.
[e]From Ref. 31. No adiabatic to isothermal correction has been carried out.

discussion). Typical integrated XRD patterns are presented in Fig. 5.

We observed that up to the maximum pressure and temperature reached (205 GPa and ~4000 K), beryllium remained in the α-Be hcp phase. New single-crystal α-Be peaks constantly appeared in the diffraction pattern at high temperature, proving a recrystallization of the hcp phase and suggesting that this phase was not metastably preserved but the actual thermodynamically stable phase in the P-T range of this study. The bcc phase should then become stable under conditions more extreme than predicted by two theoretical studies.[4,5] However, as noted in Ref. 5, the small energy difference between the hcp and bcc phases leads to large uncertainties in the predicted phase boundaries.

β-Be was not observed in the moderate pressure runs, for example, down to 8 GPa and 1225 K, which is in the stability pocket of β-Be inferred from a previous experimental report.[12] The stability field of β-Be is probably much narrower than previously thought and on the basis of our measurements, a positive α-Be to β-Be Clapeyron slope is

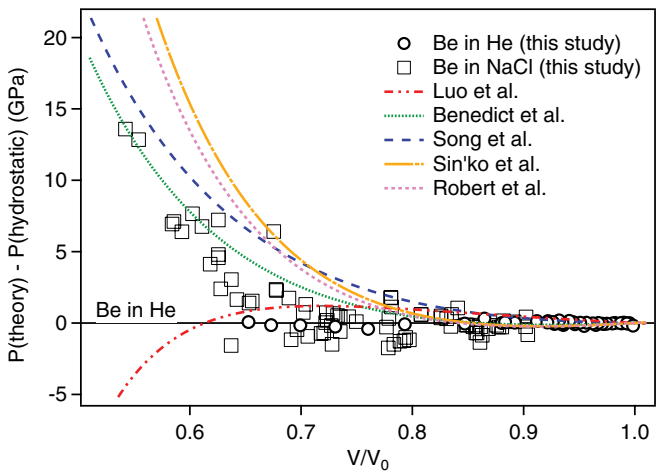

FIG. 3. (Color online) Comparison of experimental data to various theoretical models (Refs. 4,6,7,13, and 38). All curves and data show the deviation of the theoretical EoS from the optimally hydrostatic EoS determined in this study from the compression of single-crystal Be in the He medium.

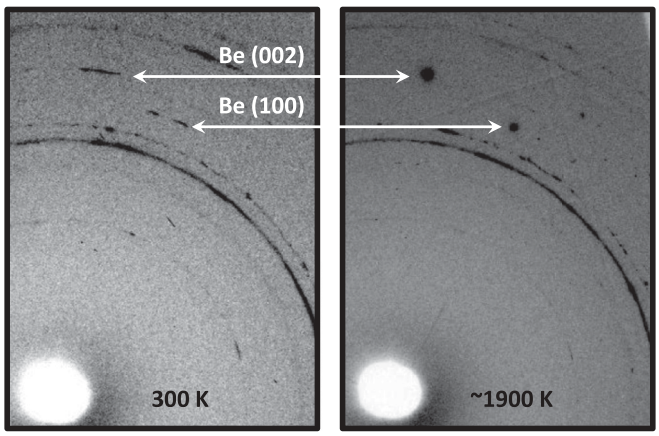

FIG. 4. X-ray diffraction patterns showing ambient T and heated beryllium diffraction peaks at ~40 GPa.

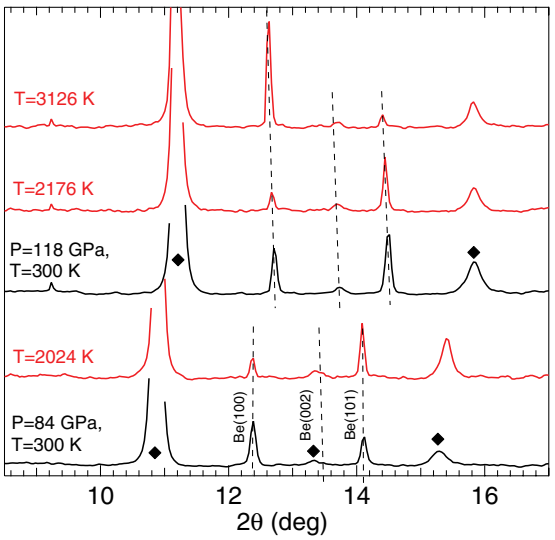

FIG. 5. (Color online) Integrated XRD patterns for Be_1 sample at two pressures. The black (red) spectra have been recorded at ambient (high) temperature. The diamonds indicate the diffraction peaks from B2-NaCl. The Be diffraction peaks are marked by dashed lines and labeled.

possible. The effect of impurities on the stability of β-Be is debated in the literature[8] and might be the cause of the apparent discrepancy between our observations and a previous report.[12]

IV. THERMAL EXPANSION UNDER PRESSURE

The data presented in this section have been obtained with the Be_4 and Be_5 samples, for which the temperature was measured by pyrometry and pressure using the MgO volume with the Ref. 21 EoS (pressure determination from NaCl in the Be_1, Be_2, and Be_3 samples is not sufficiently accurate to be included in an EoS). The P-V-T data points are listed in Table IV.

Several theoretical models have been used to predict the thermal expansion of Be in the literature: Benedict *et al.*[6] (hereafter named "Benedict") and Robert *et al.*[5] ("Robert"), Luo *et al.*[4] ("Luo"), and Song *et al.*[7] ("Song"). These models express the free energy within the Mie-Grüneisen approximation as $F(V,T) = F_0(V) + F_i(V,T) + F_e(V,T)$, where $F_0(V)$ is the static lattice component, $F_i(V,T)$ represents the contribution from ionic motion, and $F_e(V,T)$ is that from excited electrons. The electron thermal contributions have been determined to be negligible compared to the ion-thermal component in the range of interest of this study ($T \leqslant 5000$ K).[6]

$F_i(V,T)$ is estimated within the quasiharmonic (QHA) approximation for all models. For Benedict, Robert, and Luo, the parameters for this free energy are determined on the basis of the full phonon density of state calculated within GGA-PBE[5,6] or LDA.[4] For Song, they are estimated using a mean field potential approach, which deduces the Grüneisen parameter and all thermodynamic properties from the cold E(V) curve.

In the model of Benedict the ion thermal contribution to the pressure is expressed as follows:

$$P_i(V,T) = 9k_BT\left(\frac{B}{V} + A\right)\left[\frac{\theta}{8T} + \frac{1}{3}D\left(\frac{\theta}{T}\right)\right], \quad (2)$$

where $D(\theta/T)$ is the Debye function and θ is defined as

$$\theta(V) = \theta^{(0)}\left(\frac{V}{V_{\text{ref}}}\right)^{-B}\exp[A(V_{\text{ref}} - V)]. \quad (3)$$

This corresponds to the following expression for the Grüneisen parameter: $\gamma = A \times V + B$.

We have fitted the experimental P-V points with the form used by Benedict, fixing $\theta^{(0)}$ and V_{ref} to literature values: 949 K from thermodynamic measurements[20] and 8.133 Å^3/atom, respectively. The fitted A and B parameters are: $A = 0.079$ Å^{-3} and $B = 0.542$. The corresponding curves are shown in Fig. 6. This is not a unique solution, because the data are too sparse and scattered for a well-constrained fit. It can be noted, however, that the fitting parameters are very close to those of Benedict (A, B, $\theta^{(0)}$, and V_{ref} being, respectively, 0.081 Å^{-3}, 0.515, 982.8 K, and 7.75 Å^3/atom).

The thermal pressure predicted by the various models at ~1600 K is shown in Fig. 7, compared to experimental results. The Robert,[5] Luo,[4] and Benedict[6] models give similar results which agree very closely with the current experimental fit. The slope of the thermal pressure vs volume curve calculated by Song[7] is different from the three other models. However, the uncertainty of the data presented here does not allow discrimination between these two trends.

The measured thermal expansion is shown in Fig. 8 between 20 and 80 GPa and compared with the models. The 300 K values for the volume were determined from our experimental EoS. Above ~1500 K, the pressure variation during a laser heating cycle is on the order of 1 GPa, which leads to the scatter in the data in Fig. 8. Apart from this scatter the data can be considered as isobaric. The trend predicted by our high-temperature EoS is shown as the solid lines and agrees closely with the Robert,[5] Benedict,[6] and Luo[4] models. The current data are in correct quantitative agreement with the results of Song[7] as well; however, the ambient temperature thermal expansion is not reproduced well by this model. This could be due to their description of the thermodynamics of Be by a quasiharmonic model which relies only on the E(V) curve corresponding to one zero-frequency phonon. In reality beryllium has a complex phonon density of states and dispersion curves, as calculated in Refs. 5 and 6. This is demonstrated experimentally in the strong temperature dependence of the Debye temperature between 0 K and 100 K.[20]

V. MELTING BEHAVIOR

The melting curves of metals under pressure have been debated recently. The experimental melting lines of iron, as well as tantalum, molybdenum, and tungsten, differ by up to 6000 K around 300 GPa for the worst case, depending on the compression technique (static/dynamic),[44] but also the melting diagnostic. X-ray detection of melting,[45,46] based on the measurement of the diffuse x-ray signal scattered by the liquid, has called into question the conventional optical detection of melting[44,47] in laser-heated diamond anvil

TABLE IV. Lattice parameters of beryllium as a function of T measured during several heating series in Be_4 and Be_5 samples. The pressure has been calculated using MgO volume with Ref. 28 EoS. 300 K values have been fixed at the value predicted by our EoS for Be compressed in NaCl.

T (K)	MgO V (Å^3)	a (Å)	c (Å)
23.3(6) GPa (Be_4)			
300		2.164	3.414
1289	17.081	2.187	3.463
1386	17.081	2.188	3.462
1488	17.134	2.190	3.464
1544	17.145	2.191	3.473
1656	17.160	2.193	3.466
1711	17.253	2.194	3.461
1779	17.277	2.197	3.488
1926	17.362	2.204	3.462
2025	17.366	2.198	3.494
45(3) GPa (Be_4)			
300		2.088	3.301
1440	15.763	2.114	3.341
1496	15.771	2.115	3.343
1566	15.777	2.116	3.345
1643	15.808	2.117	3.338
1707	15.814	2.119	3.349
1773	15.801	2.118	3.350
1850	15.818	2.119	3.360
1970	15.858	2.122	3.352
2029	15.818	2.124	3.345
2106	15.899	2.124	3.356
2083	15.858	2.125	3.336
2156	15.865	2.123	3.351
2403	15.966	2.129	3.363
62.0(8) GPa (Be_5)			
300		2.044	3.238
1459	15.034	2.067	3.274
1580	15.055	2.068	3.277
1708	15.080	2.069	3.276
1839	15.112	2.071	3.268
1969	15.133	2.072	3.271
2111	15.165	2.074	3.275
2269	15.196	2.078	3.280
76.3(6) GPa (Be_5)			
300		2.016	3.185
1554	14.517	2.037	3.221
1661	14.506	2.037	3.224
1773	14.537	2.038	3.226
1882	14.551	2.039	3.227
2002	14.562	2.040	3.231
2129	14.601	2.043	3.234
2129	14.616	2.044	3.235
2317	14.646	2.051	3.252

T (K)	MgO V (Å^3)	a (Å)	c (Å)
30(1) GPa (Be_4)			
300		2.139	3.380
1595	16.764	2.173	3.415
1670	16.686	2.175	3.416
1927	16.813	2.173	3.422
1929	16.782	2.176	3.424
1926	16.816	2.177	3.424
2021	16.872	2.173	3.465
1489	16.694	2.166	3.406
1457	16.734	2.165	3.405
1400	16.639	2.165	3.407
1355	16.667	2.165	3.408
59(1) GPa (Be_5)			
300		2.053	3.250
1473	15.186	2.075	3.287
1618	15.202	2.077	3.293
1733	15.214	2.077	3.292
1864	15.226	2.081	3.282
67.6(9) GPa (Be_5)			
300		2.034	3.222
1517	14.823	2.052	3.242
1638	14.841	2.053	3.257
1771	14.862	2.055	3.254
1884	14.882	2.055	3.248
2003	14.919	2.054	3.269
2139	14.926	2.059	3.256
2273	14.985	2.061	3.260
82(1)GPa (Be_5)			
300		2.005	3.180
1729	14.383	2.025	3.206
1842	14.398	2.025	3.206
1937	14.405	2.026	3.208
2062	14.418	2.028	3.210
2158	14.423	2.029	3.211
2260	14.421	2.029	3.212
2260	14.430	2.030	3.213
2384	14.436	2.032	3.216
2479	14.457	2.033	3.218
2623	14.472	2.039	3.228

cells. The new diagnostic leads to higher-temperature melting points.[48,49] The XRD technique also allowed the observation of changes undergone in the laser-heated sample: thermal expansion, recrystallization from a fine powder to a few single crystals[45,48]—this phenomenon becoming faster with temperature increase[50]—but also unwanted chemical reactions between the sample and the pressure medium or the diamond anvil.[48] The onset of "fast recrystallization," evidenced by the appearance/disappearance of solid single-crystal XRD spots on each XRD pattern, has been interpreted as an evidence of

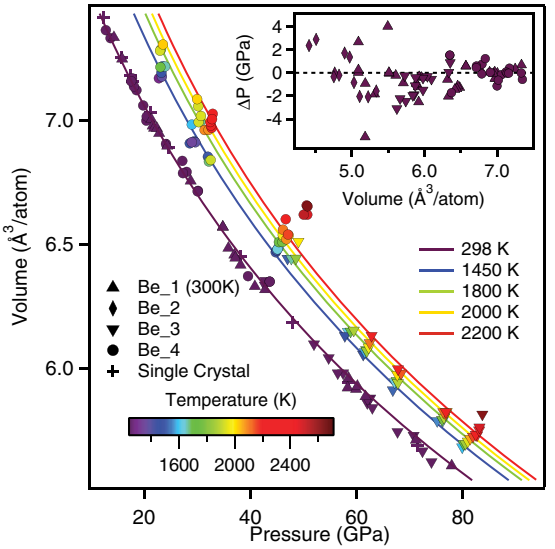

FIG. 6. (Color online) High-temperature EoS. (Inset) Deviation of experimental data from EoS fit for Be in NaCl.

melting.[50] Temperature plateaus, or decreases in slope of the temperature rise as a function of time (and laser power) are also considered as melting evidences in a few studies.[50,51]

In the case of beryllium we were able to demonstrate that fast recrystallization and changing temperature ramps do not coincide with melting. Because of the low x-ray scattering cross section of Be we failed to record a diffuse x-ray scattered signal characteristic of a liquid phase even from large samples at moderate pressure, but we did see various qualitative effects which in other studies have been correlated with melting. Over 400 K- to 1000 K-wide temperature domains below the theoretical melting point of Be (and also below the melting point of the NaCl pressure medium),[52] we observe fast recrystallization: the appearance and disappearance of single-crystal spots on each subsequent collected diffraction pattern (every 8 s during the heating ramps). Figure 9 presents the paths followed in phase space, with the regions where fast recrystallization was evident shown with red (solid) data points. The onset of fast recrystallization coincides with various changes

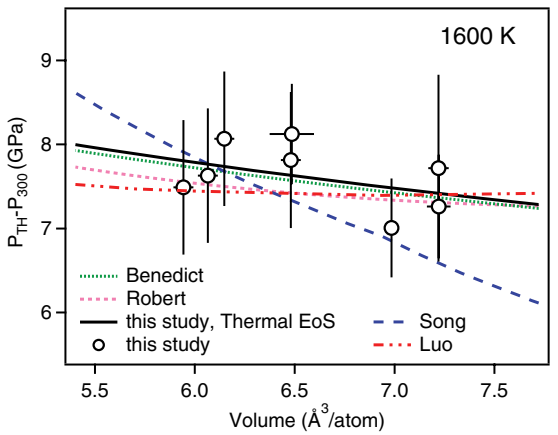

FIG. 7. (Color online) Thermal pressure at 1600 K from the various theoretical predictions (Refs. 4–7) compared to measurements made in this study.

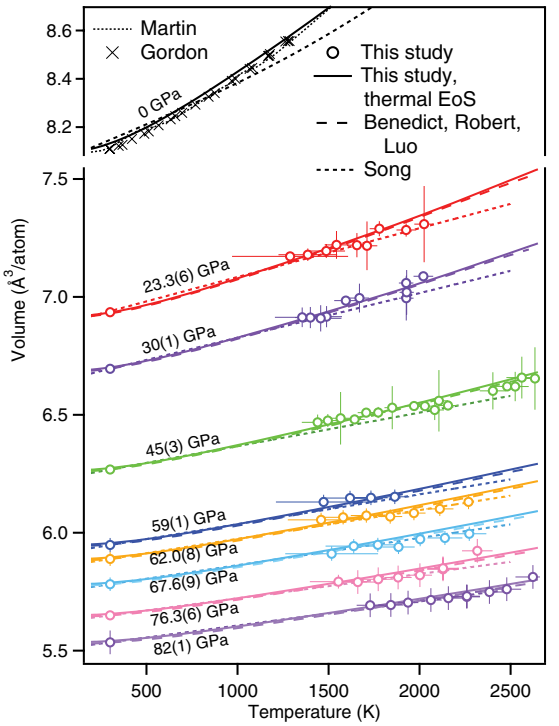

FIG. 8. (Color online) Volumetric thermal expansion, compared with theoretical models[5–7] and previous ambient pressure results.[8,19]

in the temperature ramps such as jumps, plateaus, changes of T vs time slopes or unsteady temperatures, such as the example shown in Fig. 10. Also shown in this plot is the expanding volume (calculated from observed solid diffraction peaks) as a function of temperature. It is clear that the onset of fast recrystallization and unsteadiness in the temperature

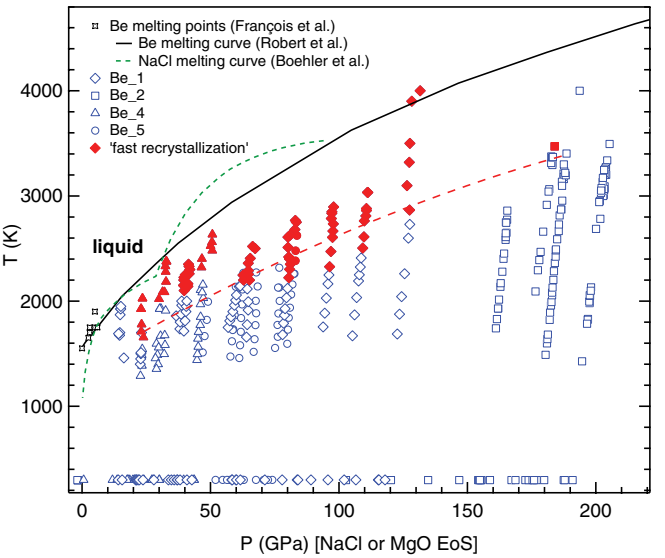

FIG. 9. (Color online) P-T conditions at which we see fast recrystallization of the beryllium samples. The red dashed line is a guide for the eye, which indicates the approximate temperature of the sample's fast recrystallization onset. The melting line predicted by Robert *et al.* (Ref. 5) and measured by Francois *et al.* are also plotted, along with melting line of the NaCl pressure medium according to Ref. 52.

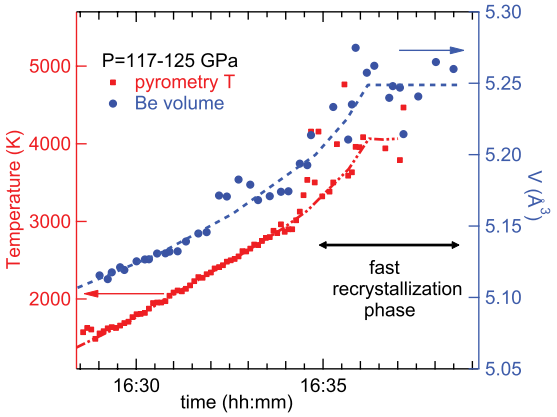

FIG. 10. (Color online) Evolution of pyrometry temperature and Be volume with time (and laser power) during one heating series for the Be_1 sample. The pressure from the NaCl EoS varied from 117 to 125 GPa. Fast recrystallization was observed between 3000 K and 4000 K, and the measured temperature was relatively unsteady during that period. The dotted lines are guides for the eye. The thermal expansion of beryllium appears to slow or stop around 4000 K, which could be an indication of melting.

ramp does not indicate melting, since the solid continues to be heated and thermally expanded above this onset temperature. It can be noted in Fig. 10 that the solid beryllium appears to stop expanding when the temperature reaches approximately 4000 K. This could be a hint of melting; 4000 K corresponds to the theoretical melting temperature. However, the data are too sparse to consider this volume plateau as a clear evidence, unlike the observation of the diffuse x-ray signal scattered by a liquid.[45] Fast recrystallization is likely to be caused by temperature-induced changes of the mechanical properties of the laser-heated solid metallic sample, such as mobility of grain boundaries. Our data on the onset of this phenomenon may be useful for benchmarking future models for mechanical properties of metals under pressure or large-scale atomistic models of the materials undergoing laser heating in a diamond anvil cell.

VI. CONCLUSION

The high pressure-temperature behavior of beryllium measured in this study has been compared with the predictions of state-of-the-art *ab initio* calculations published recently. The hcp structure (α-Be) is seen to be remarkably stable. No sign of β-Be has been observed at moderate pressure, which contradicts an experimental report[12] and calls for a revision of the stability field of this polymorph. The stability domain of the bcc phase, which is predicted to be the most stable at extreme pressures and temperatures, has not been reached in scanned range (up to 205 GPa and 4000 K). The experimental cold compression curve of the hcp α-Be up to 191 GPa reveals a slight overestimation of bulk modulus under high pressure by the generalized gradient approximation.[5–7,13] P-V-T data of hcp beryllium have been obtained in the 20- to 82-GPa and 300 K–2600 K P-T range. They can be fitted by a quasiharmonic model [Eqs. (2) and (3)] with the following parameters: $\theta^{(0)} = 949$ K, $V_{\mathrm{ref}} = 8.133$ Å^3/atom, $A = 0.079$ Å^{-3}, and $B = 0.542$. Agreement with theoretical models[5,6] based on *ab initio* phonon density of state demonstrates that Be exhibits the thermal behavior of a regular solid in this P-T range. The experimental EoS proposed here will be useful for its applications and for benchmarking future models. Rapid recrystallization of the heated sample has been observed over a wide temperature range during heating cycles and shown not to be correlated with melting in this study; our observations do not contradict the predicted melting curve under pressure.[5,6]

ACKNOWLEDGMENTS

We thank L. Benedict and T. Ogitsu for helpful discussion. We thank G. Robert, whose comments significantly improved this paper. This work was performed on the ID30 and ID27 beamlines at the European Synchrotron Radiation Facility (ESRF), Grenoble, France. Some of the work was performed under the auspices of the US Department of Energy by Lawrence Livermore National Laboratory under Contract No. DE-AC52-07NA27344.

[1] S. W. Haan, J. D. Lindt, D. A. Callahan *et al.*, Phys. Plasmas **18**, 051001 (2011).
[2] R. E. Olson, G. A. Rochau, O. L. Landen, and R. J. Leeper, Phys. Plasmas **18**, 032706 (2011).
[3] D. Swift, D. Paisley, and M. Knudon, AIP Conf. Proc. **706**, 119 (2003).
[4] F. Luo, L.-C. Cai, X.-R. Chen, F.-Q. Jing, and D. Alfe, J. Appl. Phys. **111**, 053503 (2012).
[5] G. Robert, P. Legrand, and S. Bernard, Phys. Rev. B **82**, 104118 (2010).
[6] L. X. Benedict, T. Ogitsu, A. Trave, C. J. Wu, P. A. Sterne, and E. Schwegler, Phys. Rev. B **79**, 064106 (2009).
[7] H.-F. Song and H.-F. Liu, Phys. Rev. B **75**, 245126 (2007).
[8] A. J. Martin and A. Moore, J. Less-Common Met. **1**, 85 (1959).
[9] C. W. F. T. Pistorius, in *Progress in Solid State Chemistry*, edited by J. O. McCaldin and G. Somorja, Vol. 1 (Pergamon, New York, 1976).
[10] L. C. Ming and M. H. Manghnani, J. Phys. F: Met. Phys. **14**, L1 (1984).
[11] V. Vijayakumar, B. K. Godwal, Y. K. Vohra, S. K. Sikka, and R. Chidambaram, J. Phys F: Met. Phys. **14**, 165 (1984).
[12] M. Francois and M. Contre, *Conference Internationale sur la Metallurgie du Beryllium* (Universite de France, Paris, Grenoble, 1965).
[13] G. V. Sin'ko and N. A. Smirnov, Phys. Rev. B **71**, 214108 (2005).
[14] B. Palanivel, R. S. Rao, B. K. Godwal, and S. K. Sikka, J. Phys.: Condens. Matter **12**, 8831 (2000).
[15] W. J. Evans, M. J. Lipp, H. Cynn, C.-S. Yoo, M. Somayazulu, D. Hausermann, G. Shen, and V. Prakapenka, Phys. Rev. B **72**, 094113 (2005).
[16] K. Nakano, Y. Akahama, and H. Kawamura, J. Phys.: Condens. Matter **14**, 10569 (2002).
[17] W. J. Evans *et al.*, reported in Ref. 6, unpublished.
[18] M. Boivineau, L. Arles, J. M. Vermeulen, and Th. Thevenin, Int. J. Thermophys. **14**, 427 (1993).
[19] P. Gordon, J. Appl. Phys. **20**, 908 (1949).
[20] C. A. Swenson, J. Appl. Phys. **70**, 3046 (1991).

[21]P. I. Dorogokupets and A. R. Oganov, Phys. Rev. B **75**, 024115 (2007).
[22]P. Loubeyre, R. LeToullec, D. Hausermann, M. Hanfland, R. Hemley, H. Mao, and L. Finger, Nature (London) **383**, 702 (1996).
[23]M. Mezouar, W. Crichton, S. Bauchau, F. Thurel, H. Witsch, F. Torrecillas, G. Blattmann, P. Marion, Y. Dabin, J. Chavanne, O. Hignette, C. Morawe, and C. Borel, J. Synchrotron Radiat. **12**, 659 (2005); E. Schultz *et al.*, High Press. Res. **25**, 71 (2005).
[24]L. R. Benedetti and P. Loubeyre, High Press. Res. **24**, 423 (2004).
[25]T. Sakai, E. Ohtani, N. Hirao, and Y. Ohishi, J. Appl. Phys. **109**, 084912 (2011).
[26]S. Ono, T. Kikegawa, and Y. Ohishi, Solid State Commun. **137**, 517 (2006).
[27]P. Vinet, J. R. Smith, J. Ferrante, and J. H. Rose, Phys. Rev. B **35**, 1945 (1987).
[28]P. I. Dorogokupets and A. Dewaele, High Press. Res. **27**, 431 (2007).
[29]N. Velisavljevic, G. N. Chestnut, Y. K. Vohra, S. T. Weir, V. Malba, and J. Akella, Phys. Rev. B **65**, 172107 (2002).
[30]J. F. Smith and C. L. Arbogast, J. Appl. Phys. **31**, 99 (1960).
[31]D. J. Silversmith and B. L. Averbach, Phys. Rev. B **1**, 567 (1970).
[32]L. Testardi and J. Condon, Phys. Rev. B **1**, 3928 (1970).
[33]A. Migliori, H. Lebbetter, D. J. Thomas, and T. W. Darling, J. Appl. Phys. **95**, 2436 (2004).
[34]J. P. Perdew and A. Zunger, Phys. Rev. B **23**, 5048 (1981).
[35]L. X. Benedict, private communication (2011).
[36]J. P. Perdew, K. Burke, and M. Ernzerhof, Phys. Rev. Lett. **77**, 3865 (1996).
[37]J. P. Perdew, J. A. Chevary, S. H. Vosko, K. A. Jackson, M. R. Pederson, D. J. Singh, and C. Fiolhais, Phys. Rev. B **46**, 6671 (1992).
[38]G. Robert and A. Sollier, J. Phys. IV **134**, 257 (2006).
[39]N. Tateiwa and Y. Haga, Rev. Sci. Instrum. **80**, 123901 (2009).
[40]O. L. Anderson, D. G. Isaak, and S. Yamamoto, J. Appl. Phys. **65**, 1534 (1989).
[41]K. Takemura and A. Dewaele, Phys. Rev. B **78**, 104119 (2008).
[42]U. Haussermann and S. I. Simak, Phys. Rev. B **64**, 245114 (2001).
[43]A. Dewaele, M. Torrent, P. Loubeyre, and M. Mezouar, Phys. Rev. B **78**, 104102 (2008).
[44]D. Errandonea, B. Schwager, R. Ditz, C. Gessmann, R. Boehler, and M. Ross, Phys. Rev. B **63**, 132104 (2001).
[45]A. Dewaele, M. Mezouar, N. Guignot, and P. Loubeyre, Phys. Rev. B **76**, 144106 (2007).
[46]G. Shen, V. B. Prakapenka, M. L. Rivers, and S. R. Sutton, Phys. Rev. Lett. **92**, 185701 (2004).
[47]R. Boehler, Nature (London) **363**, 534 (1993).
[48]A. Dewaele, M. Mezouar, N. Guignot, and P. Loubeyre, Phys. Rev. Lett. **104**, 255701 (2010).
[49]G. Morard *et al.*, Phys. Chem. Miner. **38**, 767 (2011).
[50]R. Boehler, D. Santamaria-Perez, D. Errandonea, and M. Mezouar, J. Phys. Conf. Ser. **121**, 022018 (2008).
[51]O. T. Lord, M. J. Walter, R. Dasgupta, D. Walker, and S. M. Clark, Earth Planet. Sci. Lett. **284**, 157 (2009).
[52]R. Boehler, M. Ross, and D. B. Boercker, Phys. Rev. Lett. **78**, 4589 (1997).